

MULTIPHYSICS MODELING OF A MAGNETIC REFRIGERATION SYSTEM BASED ON SUPERCONDUCTORS

H. R. E. H. Boucekara^{1, 2, *}, M. T. Simsim¹, M. Boucherma², and H. Allag^{2, 3}

¹Electrical Engineering Department, Umm Al-Qura University, P. Box: 5555, Makkah 21955, Saudi Arabia

²Electrical Laboratory of Constantine, LEC, Department of Electrical Engineering, Mentouri University — Constantine, Constantine 25000, Algeria

³LAMEL Laboratory, Jijel University, BP 98 Ouled Aissa, Jijel 18000, Algeria

Abstract—Based on the magnetocaloric effect, magnetic refrigeration at room temperature has, for the past decade, been a promising and environmentally friendly technology predicted to have a significantly higher efficiency than the present conventional methods. However, to the authors' knowledge, so far no prototypes have been presented for large scale applications. This paper presents the modeling of a superconducting-based magnetic refrigeration system for large scale applications. On one hand, electromagnetic computations are undertaken to maximize magnetic field produced in order to get the best performance (temperature span and cooling power) and to limit the mechanical efforts (forces and torque). On the other hand, the thermal modeling aims to evaluate and to optimize the cooling performance.

1. INTRODUCTION

Modern society very much relies on readily available cooling systems. Magnetic refrigeration (MR) has become a promising competitive technology to the conventional gas-compression/expansion technique in use today [7]. MR is a more compact and highly reliable technology.

Received 16 November 2011, Accepted 11 January 2012, Scheduled 18 February 2012

* Corresponding author: Housseem Rafik El Hana Boucekara (boucekara.housseem@gmail.com).

Furthermore, since it does not employ a compressor (which is the most inefficient part of the conventional refrigeration), it is a highly efficient technology. In addition, it is environmentally safe because only water and solid materials are used, whereas chlororoflouorocarbon refrigerants used in the conventional refrigeration may induce many harmful effects, such as toxicity, ozone depletion, and global warming hazard [10]. MR is based on magneto-caloric effect (MCE), defined as the response of a solid, i.e., change in temperature, to an applied magnetic field. When these materials are placed in a magnetic field, their temperature increases. On the other hand, when they are removed from the magnetic field, they cool down [4].

From the definition of MCE, it is clear that MR systems operate by submitting a magnetocaloric material (MCM) to a magnetic field varying between a high level and a low level with $\Delta B = B_{high} - B_{low}$. Thus, performance and efficiency of such systems depend on the level of ΔB [5]. Table 1 shows the adiabatic temperature rise under a magnetic field representing the MCE of gadolinium, as presented by [11]. These values correspond to the maximum adiabatic temperature change from this reference. As can be seen, the higher the magnetic field is, the higher the temperature changes.

There are basically three different types of magnets that can be used in a magnetic refrigeration device: the electromagnet, permanent magnet and superconducting magnet [3]. Let's now compare these three options for magnetic refrigeration systems dedicated to large scale applications.

Generating a 1 T magnetic flux density over 30 mm air gap using an iron cored solenoid with $\mu_r = 4000$ would need 24000 ampere windings. An electromagnet having 24000 ampere windings would need a massive power supply and an equally massive cooler to prevent the

Table 1. Temperature rise in the magnetic material as a function of the magnetic field [11].

Magnetic Field Change, ΔB (T)	Adiabatic Temperature Rise, ΔT (K)
1	2
2	4
3	6
5	11.6
7.5	16
10	19.3

solenoid from melting. Based on this simple evaluation, we can rule out electromagnets as applicable to large scale applications.

Let's consider now the second option, i.e., permanent magnets. At present, a great number of magnetic refrigeration permanent magnet-based devices have been built and examined, with focus on the produced temperature span and cooling power of the devices. See [2] for a review.

The magnetic flux density generated across an air gap by a permanent magnet depends on the remanence of the magnet, which is typically of the order of 1.2–1.4 T for NdFeB magnets, and the magnetic circuit, in which the magnet is placed. As the permanent magnets provide a constant magnetic flux density, they are ideal to be used for common household magnetic refrigeration applications with low power consumption [3, 6]. Nevertheless, systems using permanent magnets as source of the magnetic field (even with configurations that have specific concentration of magnetic field) are still limited to small level of magnetic field (i.e., around 2 T). Taking into account the current performance of available MCM, permanent magnet systems are used to produce low and medium power cooling (few hundred watts to several kilowatts). This can obviously change in future because of advances in research on MCM. Thus they are ruled out for large scale applications.

Having considered the electromagnet and permanent magnet and ruled out both of these options for large scale magnetic refrigeration, we will now consider superconducting magnet. It is obvious that the superconducting magnet is a better option than the traditional electromagnet as it requires little power to operate once the electromagnet has become superconducting as no power is lost to ohmic resistance. Moreover, superconducting magnet can create magnetic flux densities of the order of 5 to 10 T. Desired cooling powers for these systems can reach tens or even hundreds of kilowatts. For example, MCE and cold intrinsic power per cycle under 10 T for the Gadolinium are respectively about 20 k and 5 kJ/kg as shown in Table 1. Thus for large scale applications, e.g., large refrigerators for warehouses etc., a superconducting magnet is the best option.

In this paper, a superconducting magnet-based magnetic refrigeration system for large scale applications is considered, and a multiphysics investigation is performed.

The outline of this paper is as follows. The current section gives an introduction to different issues in magnetic refrigeration systems for large scale applications. We provided a comparison between the three main types of magnets and established the suitability of superconducting magnet in magnetic refrigeration for large scale applications. Section 2 introduces the magnetocaloric effect and

its application to produce cold. Section 3 describes the proposed structure and gives its principle of working. Section 4 presents the electromagnetic modeling of the proposed system using the finite element method and provides results from this study. In Section 5, the thermal modeling of the proposed system is explained. Results from the thermal study are also presented and discussed in detail in this section. Finally, the overall chapter conclusion is drawn in Section 6.

2. THE MAGNETOCALORIC EFFECT

2.1. Definition

As said earlier, the “magnetocaloric effect” is an intrinsic property of magnetic materials and consists of absorbing or emitting heat by the action of an external magnetic field [11]. This results in warming or cooling (both reversible) the material as shown in Figure 1.

2.2. Thermodynamic Approach

The specific entropy, which is a function of temperature and induction in the magnetocaloric material, is a combination of the magnetic entropy, the entropy of the lattice, and the entropy of the conduction electrons (assumed negligible). It is given by the following equation:

$$S(T, B) = S_m + S_L \quad (1)$$

In magnetocaloric materials, a significant variation of the entropy can be observed by the application or removal of an external magnetic field. The MCE then depends only on the initial temperature of the material and the magnetic field. The MCE can be interpreted as the isothermal entropy change or the adiabatic temperature change.

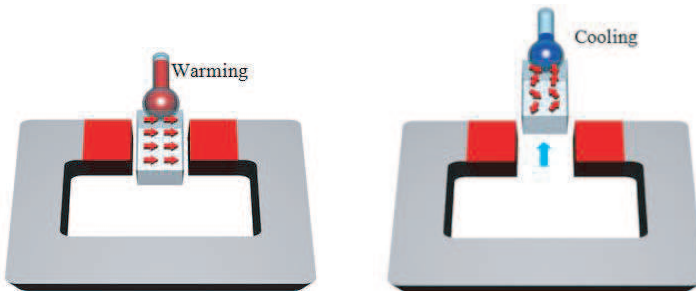


Figure 1. Magnetocaloric effect (the arrows symbolize the direction of the magnetic moments).

The separation of entropy into three terms given in (1) is valid only for second order phase transition materials characterized by a smooth variation of the magnetization as a function of temperature. For first order transitions (abrupt change of magnetization around the transition temperature), this separation is not accurate [9]. For most applications, it is sufficient to work with the total entropy which — in its differential form — can be given as:

$$dS(T, B) = \left(\frac{\partial S}{\partial T}\right)_B dT + \left(\frac{\partial S}{\partial b}\right)_t dB \quad (2)$$

The heat capacity of the material is given as:

$$C_B = \left(\frac{\partial S}{\partial T}\right)_B T \quad (3)$$

This gives:

$$\left(\frac{\partial S}{\partial T}\right)_B = \frac{C_B}{T} \quad (4)$$

From (2) and (4), we can write:

$$dS(T, B) = \frac{C_B}{T} dT + \left(\frac{\partial S}{\partial B}\right)_T dB \quad (5)$$

In the case of an adiabatic process (no entropy change $\Delta S = 0$), the formula for temperature will be written as:

$$dT = -\frac{T}{C_B} \left(\frac{\partial S}{\partial B}\right)_T dB \quad (6)$$

Using the Maxwell relation given as:

$$\left(\frac{\partial S}{\partial B}\right)_T = \left(\frac{\partial M}{\partial T}\right)_B \quad (7)$$

where M ($A\ m^{-1}$) is the magnetization.

We can write:

$$dT = -\frac{T}{C_B} \left(\frac{\partial M}{\partial T}\right)_B dB \quad (8)$$

The magnetocaloric effect (the adiabatic variation in temperature) can then be expressed as follows:

$$\Delta T_{ad} = - \int_{B_i}^{B_f} \frac{T}{C_B} \left(\frac{\partial M}{\partial T}\right)_B dB = MCE \quad (9)$$

In the case of an isothermal process, the temperature does not change during the magnetization, and we can express the entropy as:

$$dS(T, B) = \left(\frac{\partial S}{\partial B} \right)_T dB \quad (10)$$

Using the Maxwell relation given by (7), the magnetic entropy change can be expressed as:

$$\Delta S = \int_{B_i}^{B_f} \left(\frac{\partial M}{\partial T} \right)_B dB \quad (11)$$

and the heat saved in this way is transferred to the lattice thermal motion.

2.3. Theoretical Approach of MCE: Molecular Field Theory

The theoretical calculation of the MCE is based on the model of Weiss (MFT: Molecular Field Theory) and the thermodynamic relations [8]. To interpret quantitatively the ferromagnetism, Weiss proposed a phenomenological model in which the action of the applied magnetic field B was increased from that of an additional magnetic field proportional to the volume magnetization density B_v as:

$$B_v = \lambda \mu_0 M \quad (12)$$

The energy of a magnetic moment is then:

$$E = -\mu(B + B_v) \quad (13)$$

The magnetic moments will tend to move in the direction of this new field. Adapting the classical Weiss-Langevin classical calculations to a system of quantum magnetic moments, one finds:

$$M(x) = n g_J \mu_B B_J(x) \quad (14)$$

where:

$$x = \frac{J g_J \mu_B (B + \lambda \mu_0 M(x))}{k_B T} \quad (15)$$

and

$$B_J(x) = \frac{2J + 1}{2J} \coth \left(\frac{2J + 1}{2J} x \right) - \frac{1}{2J} \coth \left(\frac{1}{2J} x \right) \quad (16)$$

where: J (N m s) is the total angular momentum, n (mol^{-1}) the Avogadro number, g_J the Landé factor, μ_B (J T^{-1}) the Bohr magneton, k_B (J K^{-1}) the Boltzmann constant, $B_J(x)$ the Brillouin function, λ the Weiss molecular field coefficient, and μ_0 (T m A^{-1}) the Permeability of vacuum.

The magnetic entropy is given by the relationship of Smart [1]:

$$S_m(x) = R \left(\ln \left(\sinh \left(\frac{2J+1}{2J}x \right) / \sinh \left(\frac{1}{2J}x \right) \right) - xB_J(x) \right) \quad (17)$$

The lattice contribution can be obtained using the Debye model of phonons [1] and given by the following equation:

$$S_L = R \left(-3 \ln \left(1 - e^{-\frac{T_D}{T}} \right) + 12 \left(\frac{T}{T_D} \right)^3 \int_0^{\frac{T_D}{T}} \frac{y^3}{e^y - 1} dy \right) \quad (18)$$

where: T_D (K) is the Temperature of Debye and R ($J K^{-1}mol^{-1}$) the universal gas constant.

2.4. Application of MFT to Gadolinium Gd

In this section, the theoretical study based on the MFT developed in the previous section is applied to the gadolinium. Table 2 gives the parameters used to calculate the magnetocaloric properties.

The numerical solution of Equations (14), (15) and (16) allows getting the isotherms of magnetization and its evolution as a function of temperature calculated by the method of Weiss as shown in Figure 2(a) and Figure 2(b). Figure 2(c) represents the total heat capacity calculated from the equation (3) for different levels of induction. The magnetic entropy and its variation with temperature are shown respectively in Figure 2(d) and Figure 2(e). Finally, Figure 2(f) shows the magnetocaloric effect calculated by the MFT.

Table 2. Parameters used for applying MFT to the gadolinium.

Name	Description	Value
J	Total angular momentum	3.5
n	Avogadro number	$6.023 \cdot 10^{23}$
g_J	Landé factor	2
μ_B	Bohr magnetron	$9.2740154 \cdot 10^{-24}$
k_B	Boltzmann constant	$1.380662 \cdot 10^{-23}$
μ_0	Permeability of vacuum	$4\pi \cdot 10^{-7}$
T_C	Transition temperature	293.5
T_D	Debye temperature	184

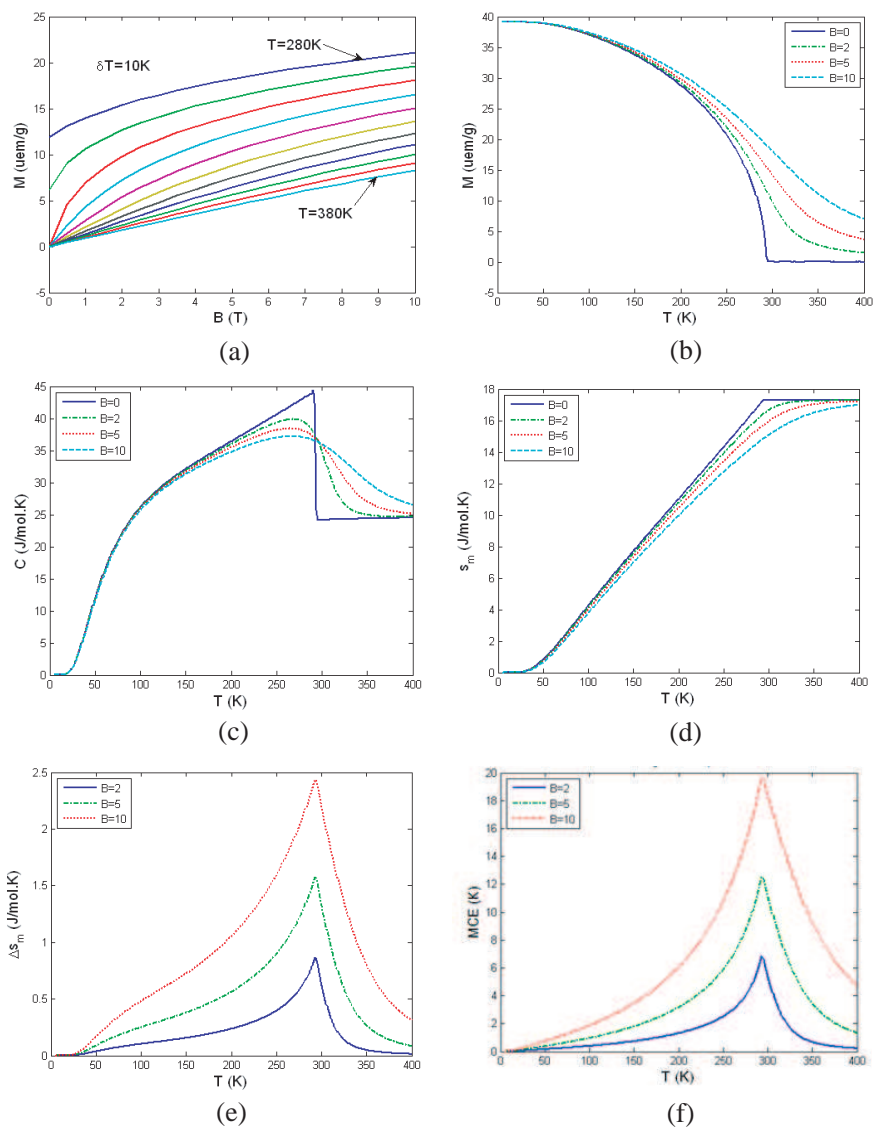


Figure 2. Results of the theoretical study applied to Gd. (a) Variation of magnetization versus the Magnetic field. (b) Variation of magnetization versus the temperature. (c) Evolution of the total heat capacity as a function of temperature. (d) Magnetic entropy. (e) Variation of the magnetic entropy. (f) MCE of Gd calculated by the MFT.

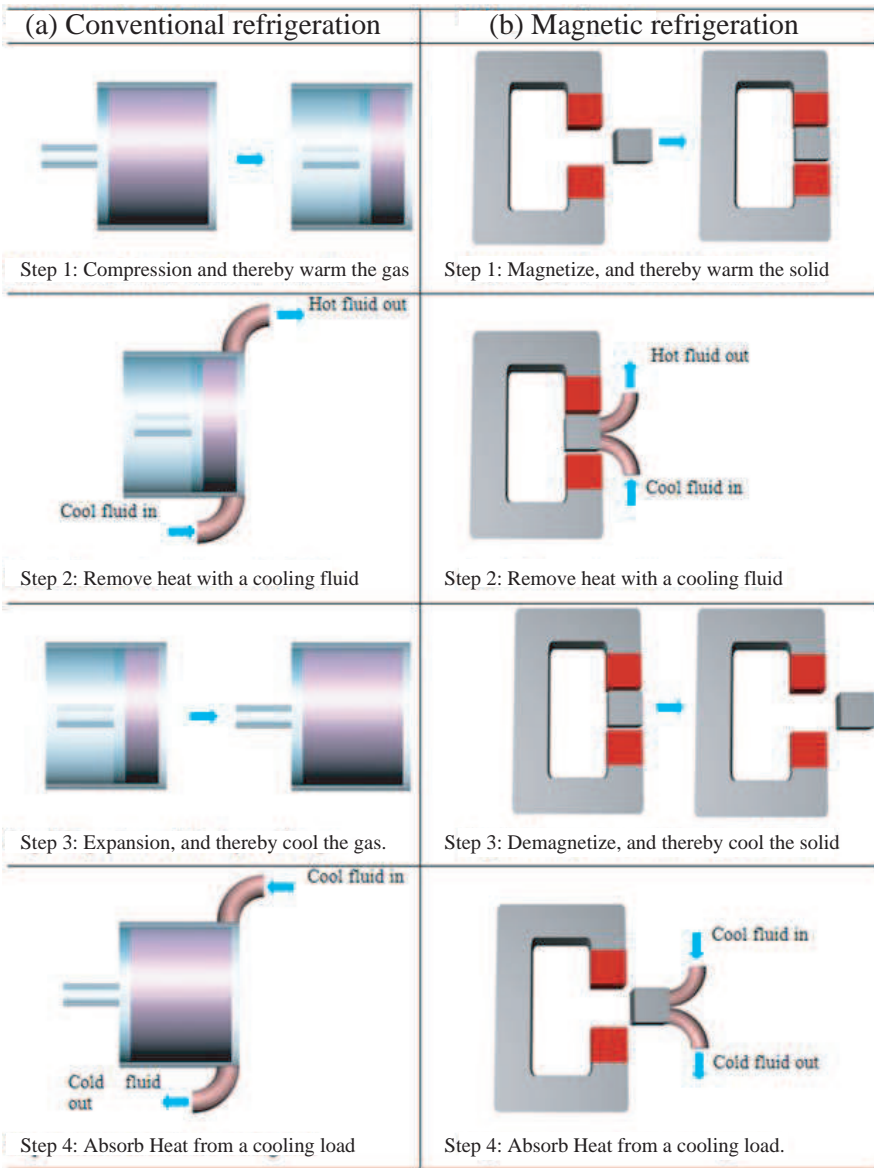


Figure 3. Analogy between magnetic refrigeration and conventional refrigeration.

2.5. Application of MCE to Produce Cooling

The magnetic cycles are generally composed of the process of magnetization and demagnetization, in which heat is discharged or

absorbed in four steps as depicted in Figure 3. From thermodynamic point of view, the magnetic cooling can be realized by: Carnot, Stirling, Ericsson and Brayton, where the Ericsson and Brayton cycles are believed to be the most suitable for such “medium or room temperature” cooling. Such cycles are predisposed to yield high cooling efficiency of the magnetic materials [4].

Figure 3(a) shows the conventional gas compression process driven by continuously repeating the four different basic processes shown, while Figure 3(b) shows the comparison of magnetic refrigeration cycles. The steps of the magnetic refrigeration process are analogous to those of the conventional refrigeration. By comparing (a) with (b) in Figure 3, we can see that the compression and expansion are replaced by adiabatic magnetization and demagnetization, respectively. These processes change the temperature of the material, and heat may be extracted and injected just as in the conventional process.

3. CONFIGURATION AND WORKING PRINCIPLE

The proposed structure is original and innovative. It is used for systems with direct magnetic refrigeration cycle where the MCM plays two main roles. First, it produces cold (due to the magnetocaloric effect), then it plays the role of a heat exchanger to exchange the produced

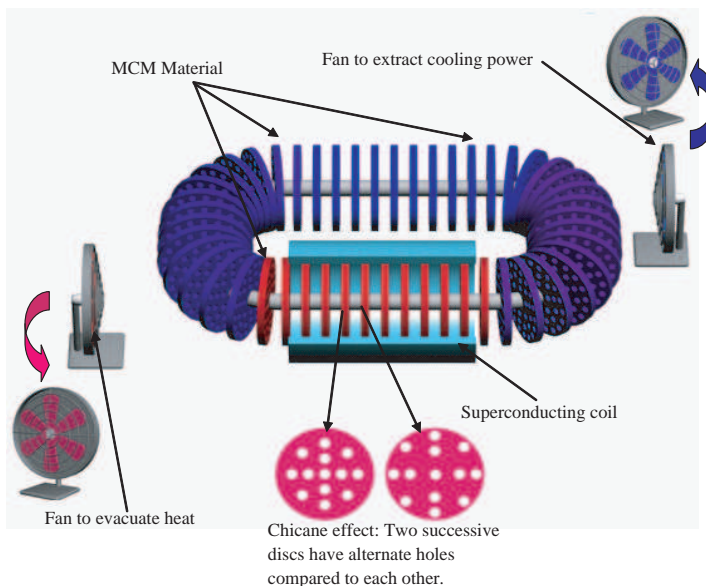


Figure 4. Configuration of the proposed system.

cold. The proposed structure consists of a superconducting coil to generate the magnetic field and N MCM cylindrical disks to produce cold. Discs turn following an elliptical track as shown in Figure 4. This structure has two fans. The first one is used to evacuate the heat generated when the MCM disks are magnetized, and the second one is used to extract the cooling power produced when the discs are demagnetized as shown in Figure 4. Discs containing the MCM include holes to facilitate heat exchanges with the air. Moreover, two successive discs have alternate holes compared to each other as illustrated in Figure 4. This helps to have a chicane effect suitable for high thermal convection exchanges. The discs track can take two forms: circular or elliptical. The choice of an elliptical one is made to increase the heat exchange between the disc and air. A second advantage by choosing an elliptical track rather than a circular one is to have a cylindrical form of the superconducting magnet. Otherwise, the superconducting magnet has to have a bend which will add more complexity to the system.

4. ELECTROMAGNETIC MODELING

In order to determine the magnetic characteristics of the proposed structure, it has been simulated using the finite element method in three dimensions via the commercial software Flux 3D. The discs in the studied structure are filled with an isotropic bulk gadolinium material with a relative permeability of 5. No eddy current or hysteresis is

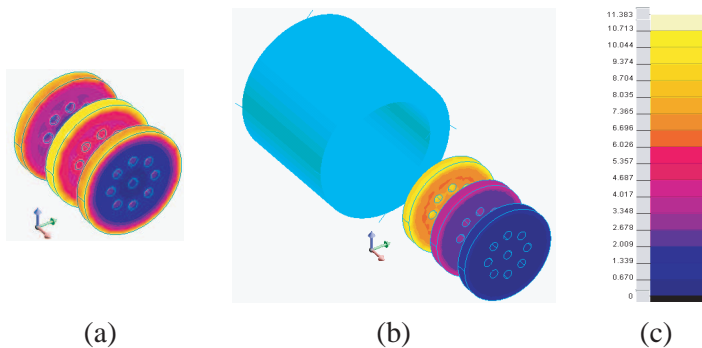


Figure 5. Induction level distribution on a portion of the system at two positions (a) inside the magnet and (b) outside the magnet. The superconducting coil is hidden in (a) for visualization purposes only. (a) The MCM discs inside magnet. (b) The MCM discs outside magnet. (c) The level of induction.

considered. The MCM discs have a radius $Rd = 110$ mm and a thickness $ed = 25$ mm. The holes inside the discs have a radius $Rh = 10$ mm. The spacing between discs is $Dd = 20$ mm (i.e., the distance between two successive discs). The superconducting magnet has an inner radius $Ri = 120$ mm, an outer radius $Re = 190$ mm and the length is $L = 300$ mm. and the current density is $J = 100$ A/mm². It operates at cryogenic temperatures (i.e., at -269 C or 4 K). The superconducting wire used is made of a Niobium-Titanium alloy.

Figure 5 shows the induction level distribution on a portion of the system at two positions. The first position corresponds to the case where the MCM discs are inside the magnet (Figure 5(a)) and the second one is when the MCM disks are outside the magnet (Figure 5(b)).

When a disc is inside the superconducting magnet, it is under to the magnetic field created by this magnet and consequently magnetized. Inversely, when the same disc is outside the magnet it is not submitted to the magnetic field and it undergoes the demagnetization phase. Hence, each disc when rotating is alternatively magnetized and demagnetized as shown in Figure 6. Moreover, since there are N discs rotating, the magnetized and demagnetized cycle is continuous for the whole structure. Thus, at any time the proposed system is producing cold.

Figure 6 shows the sketch of the induction inside 4 discs as function of the displacement. We note that each disc undergoes the magnetization and demagnetization cycle. The induction level in the centre of each disc varies from 9 T to 0 T (thus, $\Delta B = 9$ T). It is obvious that the induction is maximum for each disc when it is in the middle of the magnet. The computation at different points of the MCM showed

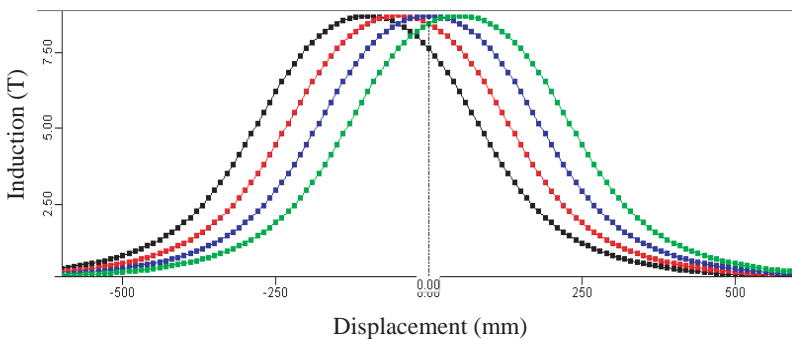


Figure 6. Induction (T) in the MCM discs as a function of displacement (mm).

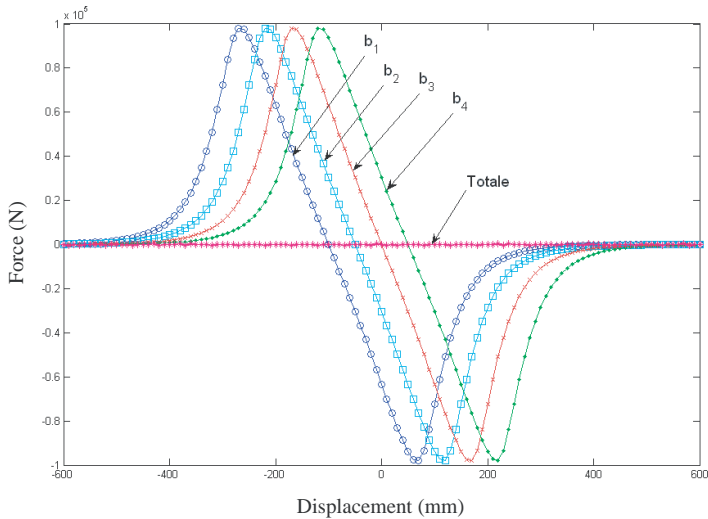


Figure 7. Forces (N) on MCM discs as a function of the displacement (mm).

that the average disc induction is almost the same as its average value taken in the disc centre. The difference observed is less than 5%.

Figure 7 sketches the forces exerted on 4 successive discs. The magnetic forces vary with the displacement. Their maximum value is about $1e5 N$. If the distance between the discs is optimized with respect to the dimensions of the discs, the resulting total force which is the sum of the forces on all disks is almost zero as shown in Figure 7.

5. THERMAL MODELING

5.1. Formulation

The energy balance for a solid in convective heat exchange with an external fluid indicates that the decrease in internal energy is equal to the heat transferred by convection. Thus:

$$-q_{int} = q_{conv} \tag{19}$$

The decrease in internal energy is given by:

$$q_{int} = mC \frac{dT}{dt} = \rho \vartheta C_p \frac{dT}{dt} \tag{20}$$

where m (kg) is the solid mass, C ($J\ kg^{-1}K^{-1}$) is the specific heat and ϑ (m^3) is the solid volume.

The temperature of the solid varies only with time $\frac{\partial T}{\partial t}$. The heat transferred by convection is given by:

$$q_{conv} = hS(T - T_{\infty}) \quad (21)$$

where: S (m^2) is the heat exchange surface and T_{∞} [K] is the fluid temperature.

The initial conditions are given by the following equation:

$$t = 0, \quad T = T_{initial} \quad (22)$$

Combining Equations (19), (20) and (21) gives:

$$-\rho V C_p \frac{dT}{dt} = hS(T - T_{\infty}) \quad (23)$$

To simplify this differential equation, we introduce the following variable:

$$\theta = \frac{T - T_{\infty}}{T_i - T_{\infty}} \quad (24)$$

Thus, the derivative with respect to time is given by:

$$\frac{\partial T}{\partial t} = (T_i - T_{\infty}) \frac{\partial \theta}{\partial t} \quad (25)$$

The substitution of (25) in (23) gives:

$$-\rho V C_p = (T_i - T_{\infty}) \frac{\partial \theta}{\partial t} = hS(T - t_{\infty}) \quad (26)$$

Thus:

$$-\frac{\rho V C_p}{hS} \frac{d\theta}{dt} = \theta \quad (27)$$

For integration we can write (27) as:

$$-\frac{d\theta}{\theta} = \frac{\rho V C_p}{hS} dt \quad (28)$$

The temperature inside the solid varies between T_1 at $t = t_1$ and T at any time $t > t_1$. Thus, θ varies between θ_1 and θ_2 . We can write:

$$-\int_{\theta_1}^{\theta} \frac{d\theta}{\theta} = \frac{hS}{\rho V C_p} \int_{t_1}^t dt \Rightarrow -(\ln(\theta) - \ln(\theta_1)) = \frac{hS}{\rho V C_p} (t - t_1) \quad (29)$$

The final solution then is given by:

$$\frac{\theta}{\theta_1} = \exp \left[- \left(\frac{hS}{\rho V C_p} \right) (t - t_1) \right] \quad (30)$$

The quantity $\alpha = \left(\frac{\rho \theta C_p}{hS} \right)$ is called the thermal time constant for a given geometry.

We have $\theta_1 = \frac{T_1 - T_\infty}{T_i - T_\infty}$ and $\theta = \frac{T - T_\infty}{T_i - T_\infty}$, thus we can write the expression of the temperature in function of the time as follow:

$$T(t) = (T_1 - T_\infty) \exp\left(-\frac{1}{\alpha}(t - t_1)\right) + T_\infty \quad (31)$$

Observe from Equation (31) that the smaller the time constant is, the more rapidly the temperature decreases, i.e., the faster the response. This is illustrated in Figure 8. A system with a small time constant gives a fast response in that it reaches the steady state (or final state) quickly due to quick dissipation of energy stored, whereas a system with a large time constant gives a slow response because it takes longer to reach steady state.

Combining Equations (21) and (31) allows us to write the expression of instantaneous energy as follow:

$$q(t) = hS(T_\infty - T_i) \exp\left(-\frac{1}{\alpha}(t - t_1)\right) \quad (32)$$

The integration of the instantaneous energy over a time interval,

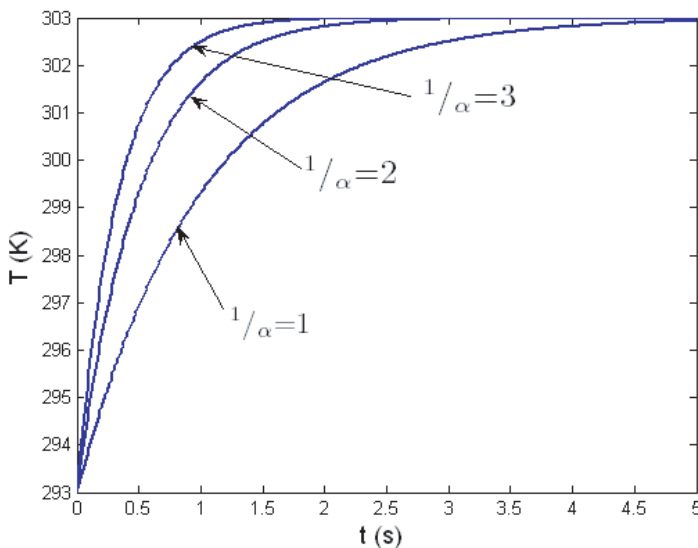


Figure 8. Plot of the temperature for various values of the time constant.

gives the total energy:

$$Q = \int_{t_1}^t q dt \Rightarrow Q = \rho \vartheta C_p (T_\infty - T_i) \left\{ 1 - \exp \left(-\frac{1}{\alpha} (t - t_1) \right) \right\} \quad (33)$$

Initialization :	
<ul style="list-style-type: none"> - Inputs (geometrical and physical parameters): MCM specific heat, air specific heat, period, air density, MCM density, air viscosity, thermal conductivity, air velocity, room temperature, MCE, number of cycles number of time calculation steps per cycle, etc. - Initial conditions. - Calculation of intermediate parameters: Nusselt, Reynolds and Prandtl numbers, the heat transfer coefficient etc. 	
For $k= 1:1: N_c$ (Number of cycles)	
Step 1: Magnetization of the MCM causing an increase in its temperature.	
	$t = t_0 : \delta t : t_1$ $T_1(t) = T(t_0) + MCE$ $Q_1 = \rho VC_p (T_1(t_1) - T_1(t_0)) (t_2 - t_1) = \rho VC_p EMC \cdot (t_2 - t_1)$
Step 2: Heat exchange with the hot source.	
	$t = t_1 : \delta t : t_2$ $T_2(t) = (T_1(t = t_1) - T_{f\infty}) \exp \left(-\frac{1}{\alpha} (t - t_1) \right) + T_{f\infty}$ $Q_2 = \rho VC_p (T_2(t_2) - T_2(t_1)) \left\{ 1 - \exp \left(-\frac{1}{\alpha} (t_2 - t_1) \right) \right\}$
Step 3: Demagnetization of the MCM causing a decrease in its temperature.	
	$t = t_2 : \delta t : t_3$ $T_3(t) = T_2(t_2) - MCE$ $Q_3 = \rho VC_p (T_3(t_3) - T_3(t_2)) (t_3 - t_2) = \rho VC_p EMC \cdot (t_3 - t_2)$
Step 4: Heat exchange with the cold source.	
	$t = t_3 : \delta t : t_4$ $T_4(t) = (T_3(t_3) - T_{c\infty}) \exp \left(-\frac{1}{\alpha} (t - t_3) \right) + T_{c\infty}$ $Q_4 = \rho VC_p (T_4(t_4) - T_4(t_3)) (t_4 - t_3) \left\{ 1 - \exp \left(-\frac{1}{\alpha} (t_4 - t_3) \right) \right\}$
Time reinitialization:	
$t_0 = t_4$ $t_1 = t_0 + N_p \delta t$ $t_2 = t_1 + N_p \delta t$ $t_3 = t_2 + N_p \delta t$ $t_4 = t_3 + N_p \delta t$	
End	
Results exploitations :	
<ul style="list-style-type: none"> - Thermal characteristics (temperature, power and energy profiles). - Parametric study of the influence of parameters on the thermal characteristics. - Inverse problem identification. - Optimization. 	

Figure 9. Thermal modeling of direct cycles magnetic refrigeration.

5.2. Numerical Model

Figure 9 describes the thermal model associated with the four steps of the direct magnetic refrigeration cycle. The core of the program is independent of geometrical and physical parameters as well as the intermediate parameters giving more flexibility to the model.

Table 3. Thermal design parameters.

Name	Descriptio	Valu
ρ_{Gd}	Gadolinium density (kg/m ³)	8000
ρ_{air}	Air density (kg/m ³)	1.177
C_{Gd}	Gadolinium pecific heat (J kg ⁻¹ K ⁻¹)	23
C_{air}	Air specific heat (J kg ⁻¹ K ⁻¹)	1005.7
B	Induction (T)	9
Nc	Number of cycles	20
Np	Number of time calculation steps per cycle	
Ta	Room temperature (k)	29
V	Air velocity (m/s)	10
ν	Air viscosity (m ² /s)	15.68e-6
λ	Thermal conductivity (W/(m·K))	0.0262
τ	Period (s)	1

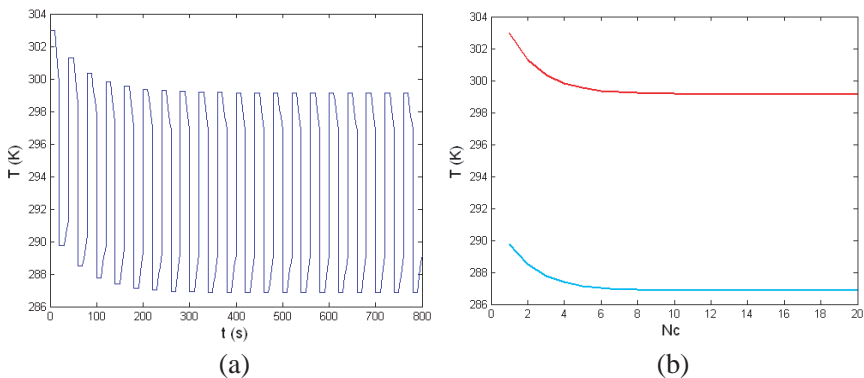


Figure 10. (a) Evolution of the material temperature profile over time. (b) Envelope of the temperature profile of the material versus to the number of cycles.

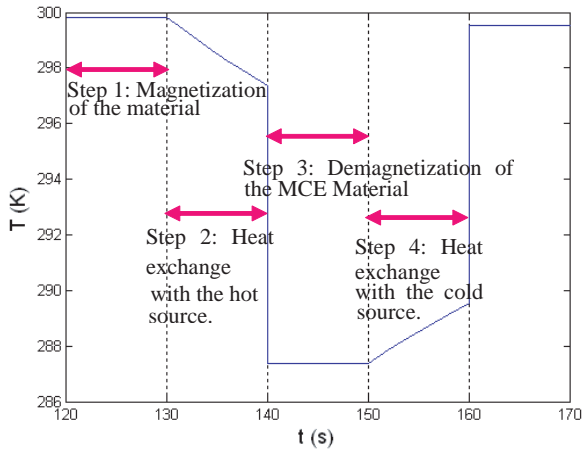


Figure 11. Schematic representation of the four phases of a direct magnetic refrigeration cycle zoomed from Figure 10.

5.3. Application and Results

The developed thermal model has been applied to the proposed structure. In addition to the geometric parameters described before, the thermal design parameters are given in Table 3.

Figure 10(a) shows the temperature profile of the MCM discs (during the four phases that we have represented in Figure 11) versus time. Figure 10(b) shows the evolution of the temperature of the MCM at the end of each cycle performed. As mentioned earlier the energy is produced and exchanged through the MCM discs.

6. CONCLUSIONS

A new and original superconductor magnet-based magnetic refrigeration system has been proposed for large scale applications. A multiphysics modeling has been investigated to evaluate the performance of such system. An electromagnetic modeling has been achieved to compute the magnetic field created by the magnet, and a $\Delta B = 9$ T has been found. From the definition of the MCE, this magnetic field is greatly linked to the performance of the system. However, the produced magnetic efforts are very important. An optimization of the spacing between the discs has reduced the resulting force considerably. The thermal modeling has been carried out to estimate the cooling performance, i.e., the cooling energy and temperature span produced by the system. In this work, the cooling performances of the designed system are $\Delta T = 13$ K and $Q = 2500$ J for the chosen parameters.

REFERENCES

1. Allab, F., "Conception et réalisation d'un dispositif de réfrigération magnétique basé sur l'effet magnétocalorique et dédié à la climatisation automobile," Thèse de doctorat, Grenoble, Institut National Polytechnique de Grenoble, 2008.
2. Bjørk, R., Bahl, C. R. H., A. Smith, and N. Pryds, "Review and comparison of magnet designs for magnetic refrigeration," *International J. of Refrigeration*, Vol. 33, No. 3, 437–448, 2010.
3. Bjørk, R., C. R. H. Bahl, A. Smith, and N. Pryds, "On the optimal magnet design for magnetic refrigeration," *Proceedings of the 3rd International Conference on Magnetic Refrigeration at Room Temperature*, 473–480, Des Moines, Iowa, USA, 2009.
4. Bouchekara, H. R. E. H., "Recherche sur les systèmes de réfrigération magnétique. Modélisation numérique, conception et optimisation," Thèse de doctorat, Grenoble Institut National Polytechnique, 2008.
5. Bouchekara, H. R. E. H., A. Lebouc-Kedous, and J. P. Yonnet, "Electromagnetic design of a magnetic field source for a magnetocaloric refrigerator," *Progress In Electromagnetics Research M*, Vol. 19, 251–263, 2011.
6. Bouchekara, H. R. E. H., M. T. Simsim, Y. Berrouche, and M. Anwari, "Design and optimization of a permanent magnet rotating machine for power cooling generation," *Progress In Electromagnetics Research M*, Vol. 20, 57–71, 2011.
7. Bruck, E., O. Tegus, X. W. Li, et al., "Magnetic refrigeration-towards room-temperature applications," *Physica B: Condensed Matter*, Vol. 327, Nos. 2–4, 431–437, Apr. 2003.
8. Huang, W. N. and C. C. Teng, "A simple magnetic refrigerator evaluation model," *Journal of Magnetism and Magnetic Materials*, Vol. 282, 311–316, 2004.
9. Kitanovski, A. P., W. Egolf, F. Gender, O. Sari, and C. H. Besson, "A rotary heat exchanger magnetic refrigerator," *International Conference on Magnetic Refrigeration at Room Temperature*, Montreux, Switzerland, 2005.
10. Shir, F., E. Della Torre, and L. H. Bennett, "Modeling of magnetization and demagnetization in magnetic regenerative refrigeration," *IEEE Transactions on Magnetics*, Vol. 40, No. 4, 2098–2100, Jul. 2004.
11. Tishin, A. M., K. A. Gschneidner, and V. K. Pecharsky, "Magnetocaloric effect and heat capacity in the phase-transition region," *Physical Review B*, Vol. 59, No. 1, 503–511, 1999.